Time-warp correction and calibration in photonic time-stretch analog-to-digital converter

Shalabh Gupta* and Bahram Jalali

Department of Electrical Engineering, University of California, Los Angeles, 420 Westwood Boulevard, Los Angeles, California 90095, USA

**Corresponding author: shalabh@ee.ucla.edu*

Received September 9, 2008; accepted October 3, 2008;
posted October 16, 2008 (Doc. ID 101406); published November 14, 2008

We show how time warps caused by nonuniform wavelength-to-time mapping in the photonic time-stretch analog-to-digital converter (ADC) can be digitally measured and removed. This is combined with digital correction of wavelength-dependent Mach–Zehnder modulator (MZM) bias offset to attain a 10 GHz bandwidth digitizer with >7 effective bits of resolution and 52 dB spur-free dynamic range. To the best of our knowledge, this is the highest resolution ADC in 10 GHz bandwidth range, with at least 1 order of magnitude higher signal-to-noise ratio than ever achieved. We also demonstrate concatenation of 30 wavelength interleaved time segments with high fidelity on the path to achieving continuous time operation. © 2008 Optical Society of America

OCIS codes: 060.5625, 070.1170, 070.6020.

With increased bandwidth demands from the Internet backbones, researchers are targeting 100 Gbit/s and higher data rates per wavelength division multiplexing (WDM) channel using spectrally efficient, multilevel modulation formats [1]. Demodulation of such signals requires analog-to-digital converters (ADCs) with very high performance and resolution. Such ADCs are also crucial for defense applications such as radars and for wide-bandwidth laboratory instruments such as oscilloscopes and vector spectrum analyzers. However, resolution of the ADCs universally deteriorates at high frequencies because of, for example, jitter in the sampling clocks or the finite switching time of electronic comparators [2]. By reducing the rf signal frequency prior to quantization, the photonic time-stretch (TS) technique aims to overcome these limitations [3–7].

In a photonic TS-ADC, the rf signal is modulated over a linearly chirped optical pulse. It is subsequently slowed down in time when it passes through a highly dispersive medium, owing to its group velocity dispersion (GVD), before being converted back to electrical domain by a photodetector. The resulting time dilation reduces both the carrier frequency and the bandwidth of the signal. This bandwidth-compressed waveform is then quantized by an electronic digitizer that would have been too slow to capture the original signal.

Nonuniform envelope of the chirped pulse and the laser relative intensity noise reduce the TS-ADC dynamic range. Differential operation and digital post-processing reduce these effects [8,9], and arcsine operation suppresses distortion due to nonlinear MZM transfer function, as in other photonic ADC systems [10]. The obtained waveforms still suffer from another type of impairment: nonuniform mapping between the original and the stretched time scales, or a time warp, as shown in Fig. 1. This effect is caused by nonlinear wavelength-to-time mapping and originates from a multitude of sources.

The TS, or equivalently the bandwidth compression factor is given by $C=(D_1+D_2)/D_1$, where D_1 and D_2 are the dispersion values of the first and second dispersion compensating fibers (DCFs) [7]. D_1 and D_2 are wavelength dependent, but their ratio, and hence C, are wavelength independent, as long as the two fibers have matching dispersion coefficients β_2, β_3, β_4, etc. However, finite mismatches in reality cause the compression factor to be wavelength dependent (and hence time dependent by virtue of wavelength-to-time mapping), culminating in a time warp.

Wavelength division multiplexing (WDM)/demultiplexing filters have wavelength-dependent group delay variation [11] and result in additional time warps. Fortuitously, their contribution to the distortion is reduced by the compression factor if these filters are placed after the MZM, in the same way as TS helps in reducing noise due to electronic clock jitter.

Optical nonlinearity in the fiber can be yet another source time-warp distortion. The ultrafast optical pulses originating from the mode-locked laser (MLL) initially have very high peak power (in the first DCF stage), which can result in self-phase modulation (SPM) owing to optical Kerr nonlinearity [12]. If present, SPM combined with GVD can distort the de-

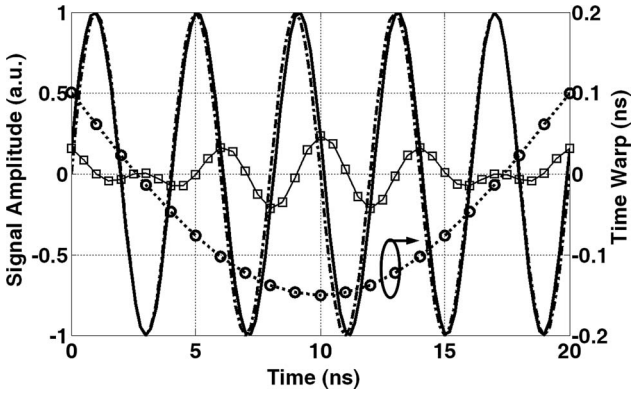

Fig. 1. Solid trace shows an ideal signal without time warp; dashed trace is a signal with time warp; trace with squares represents the error; trace with circles represents amplitude of the time warp.

0146-9592/08/222674-3/$15.00

sired linear wavelength-time mapping and result in time warps.

When waveforms from adjacent WDM channels are combined, there are small timing skews between them. Even though much of the skews can be removed in hardware by adjusting electronic clocks and delays using feedback, some residual skews remain, which effectively appear as sharp time warps at channel boundaries, as seen in Fig. 2.

The time warp due to all these effects is essentially static over time and can be corrected by a single operation. To measure it for calibration, a sinusoidal rf tone is stretched using a few hundred optical pulses and captured by slow ADCs. The waveforms from adjacent WDM channels are coarsely aligned in time and concatenated. A sinusoidal curve fit is then performed, and the difference between the measured waveforms' and ideal sine-fit curves' zero crossings (averaged over these waveforms) is obtained, as shown in Fig. 2. The sharp jump in the center shows timing skew between sinusoids from the adjacent WDM channels. These data are used to correct the time warp in unknown arbitrary signals by performing second-order polynomial interpolation. Once the averaged time-warp data are obtained, interpolation can easily be performed in real time using a dedicated digital signal processor.

Even after these operations, the signal has a time-varying second-harmonic distortion due to the wavelength-dependent MZM bias offset caused by imperfect path-length matching in the MZM [13]. This effect becomes significant for wide optical bandwidths and can be reduced to some extent with the arcsine operation itself [8]. However, estimating the bias offset from dc terms becomes difficult, as there are unknown dc offsets added by electronics, and the second-order nonlinearity generates additional dc terms. To overcome these problems and correct for nonlinearity owing to MZM bias offsets, the same sine-fitting technique is used as for time-warp correction. However, in this case, the average amplitude of the second harmonic is obtained along the time axis for the combined waveforms, as shown in Fig. 3. It is found that second-harmonic amplitude $\delta(t)$ varies linearly with the wavelength, as expected from the wavelength dependence of bias offset. Once $\delta(t)$ is

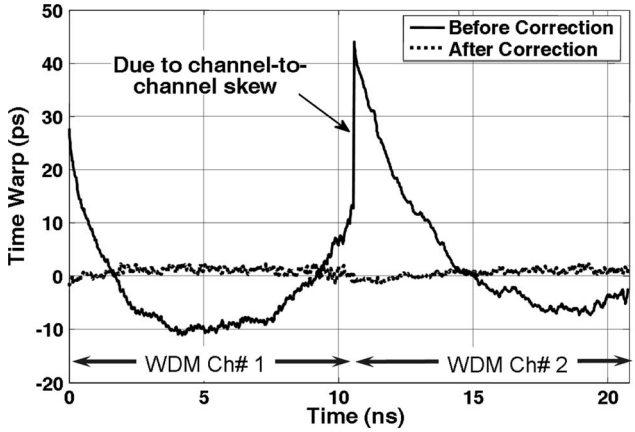

Fig. 2. Time-warp magnitudes before and after correction along the time axis of two combined WDM channels.

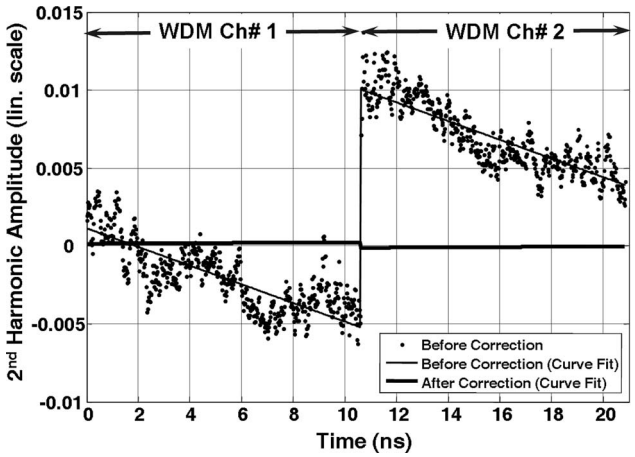

Fig. 3. Second-harmonic amplitude versus time/wavelength.

measured, the linearized signal $y(t)$ is obtained from the uncorrected signal $x(t)$ as

$$y(t) = x(t) - \delta(t)(2x^2(t) - 1). \quad (1)$$

For example, an rf signal, $\cos(\omega t)$, with time-dependent second-harmonic amplitude given by $\delta(t)$, takes the form $x(t) = [\cos(\omega t) + \delta(t)\cos(2\omega t)]$. Equation (1) gives $y(t) = [\cos(\omega t) + \text{second-order terms in } \delta(t)]$. Since $\delta(t)$ itself is small, the $\delta^2(t)$ terms become negligible, and hence original signal $y(t) \approx \cos(\omega t)$ is obtained.

Figure 4 shows the experimental setup of the TS system. Optical pulses from the MLL are sent through a 0.33 m long highly nonlinear fiber (HLNF). SPM in the fiber broadens their bandwidth from 17 nm to more than 40 nm, giving high quality supercontinuum (SC). These pulses are stretched in the first DCF with −40 ps/nm GVD to obtain chirped pulses. SC pulses are carved out from them using standard telecom 19 nm bandwidth filters at 1551 and 1571 nm wavelengths, and amplified using C-band and L-band erbium-doped fiber amplifiers (EDFAs), respectively.

In addition to amplification, the 1551 nm channel pulses are delayed, so the trailing edge of nth pulse in the L band slightly overlaps with the leading edge of $(n-1)$th pulse in the C band. This ensures continuity of the rf signal between adjacent WDM channels.

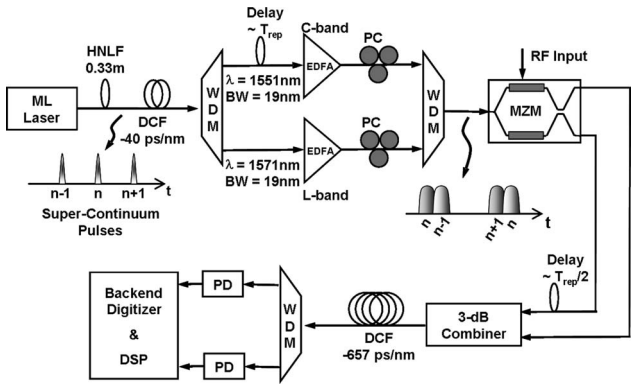

Fig. 4. Experimental setup of the system.

The overlapping L-band and C-band pulses are derived from separate laser pulses to demonstrate seamless combination of the TS signals from adjacent pulses, as required in a fully continuous operation. Polarization controllers (PC) after the EDFAs in two WDM channels independently correct for their polarizations before combining the optical pulses in the second coarse wavelength division multiplexing filter, which is followed by the intensity modulator.

The rf signal differentially modulates the optical pulses using dual output push–pull MZM [8]. For ease of implementation, the two MZM outputs are relatively skewed in time and multiplexed onto the second DCF, which has a dispersion value of −657 ps/nm, achieving a bandwidth compression factor of 17. The WDM channels at the DCF output are demultiplexed and detected using photoreceivers (with ~0.5 mW average input optical power). The obtained rf signal is digitized by a Tektronix DPO71604 oscilloscope, and further signal processing is performed on a computer.

With this setup, single- and two-tone tests were perfomed with signal frequencies varying from 4 to 16 GHz and modulation depth of ~0.7 and ~0.5, respectively. The time warps were found to be almost constant, whereas channel-to-channel timing skews had a slow variation with time.

For any signal, calibration data obtained from the first half of the captured waveforms (365 pulses in 10 μs) were applied for correcting distortions in the remaining 365 pulses. For these pulses, 10 GHz noise bandwidth gave 7.05–7.25 effective number of bits (ENOBs) on an average (obtained by sine curve fitting). For two-tone tests, signal power was reduced by 3 dB to avoid clipping, resulting in about 6.5–6.7 ENOBs (or effectively 7.0–7.2 ENOBs when referred to full-scale signal power). High-resolution bandwidth was achieved by concatenating 30 time segments synchronously, giving a worst-case spurious free dynamic range (SFDR) of 52 dB, as seen in Fig. 5 Fourier transform plots. The obtained signal-to-noise ratio was limited primarily by 7.2 ENOB resolution (over 1 GHz bandwidth) of the back-end digitizer.

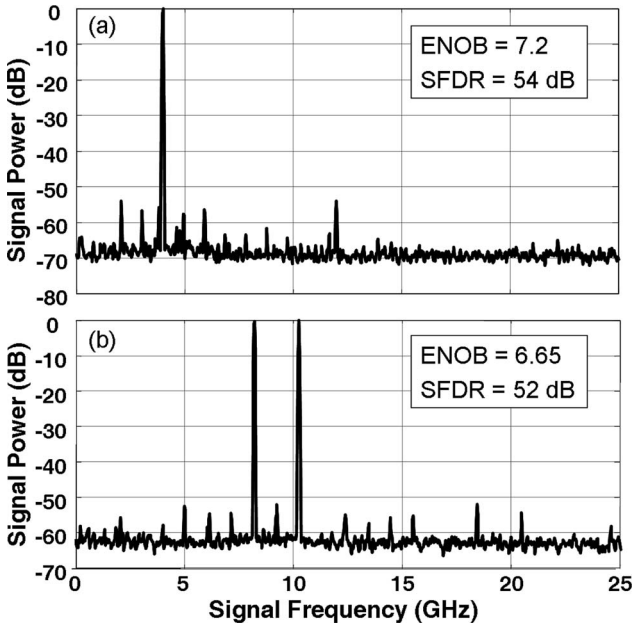

Fig. 5. (a) Single-tone test with 4 GHz rf; (b) two-tone test with 8.2 and 10.25 GHz rf signals. In both, 30 waveforms are stitched coherently to achieve high-resolution bandwidth and show scalability to a continuous system.

In conclusion, we demonstrated the capture of 10 GHz bandwidth rf signals with >7 ENOB resolution and >52 dB SFDR—a world record in ADC performance. This was made possible by use of a new powerful algorithm to correct for distortions caused by time warps and wavelength-dependent MZM bias offsets in photonic TS-ADC. We also showed a path to continuous operation by concatenating 30 time segments with high fidelity.

This work was supported by the DARPA-MTO PHOBIAC program. The authors thank George C. Valley, Gary Betts, Ozdal Boyraz, and George Seffler for highly useful discussions.

References

1. P. J. Winzer and G. Raybon, *2007 Digest of the IEEE/LEOS Summer Topical Meetings* (IEEE, 2007), pp. 7–8.
2. R. H. Walden, IEEE J. Sel. Areas Commun. **17**, 539 (1999).
3. A. S. Bhushan, F. Coppinger, and B. Jalali, Electron. Lett. **34**, 839 (1998).
4. B. Jalali and F. Coppinger, "Data conversion using time manipulation," U.S. patent 6,288,659 (September 11, 2001).
5. J. Chou, O. Boyraz, D. Solli, and B. Jalali, Appl. Phys. Lett. **91**, 161105 (2007).
6. G. C. Valley, Opt. Express **15**, 1955 (2007).
7. Y. Han and B. Jalali, J. Lightwave Technol. **21**, 3085 (2003).
8. S. Gupta, G. C. Valley, and B. Jalali, J. Lightwave Technol. **25**, 3716 (2007).
9. S. Gupta, B. Jalali, J. Stigwall, and S. Galt, *2007 IEEE International Topical Meeting on Microwave Photonics* (IEEE, 2007), pp. 141–144.
10. P. W. Juodawlkis, J. C. Twichell, G. E. Betts, J. J. Hargreaves, R. D. Younger, J. L. Wasserman, F. J. O'Donnell, K. G. Ray, and R. C. Williamson, IEEE Trans. Microwave Theory Tech. **49**, 1840 (2001).
11. G. Lenz, B. J. Eggleton, C. R. Giles, C. K. Madsen, and R. E. Slusher, IEEE J. Quantum Electron. **34**, 1390 (1998).
12. G. P. Agrawal, *Nonlinear Fiber Optics* (Academic, 2001).
13. S. Dubovitsky, W. Steier, S. Yegnanarayanan, and B. Jalali, J. Lightwave Technol. **20**, 886 (2002).